Iron substitution in NdCoAsO: crystal structure and magnetic phase diagram

Michael A. McGuire, Athena S. Sefat, Brian C. Sales, and David Mandrus

Oak Ridge National Laboratory, Oak Ridge, Tennessee 37831 USA

(Dated: September 10, 2010)

The effects of replacing small amounts of Co with Fe in NdCoAsO are reported. Polycrystalline materials with compositions $NdCo_{1-x}Fe_xAsO$ ($x = 0.05$, 0.10, 0.15, and 0.20) are studied and the results compared to previous reports for NdCoAsO. Rietveld analysis of powder x-ray diffraction data shows that as Fe replaces Co on the transition metal (T) site, the $T-As$ distance increases, and the As tetrahedra surrounding the T-site become more regular. Electrical resistivity and magnetization measurements indicate that the three magnetic phase transitions in NdCoAsO are suppressed as Co is replaced by Fe, and these transitions are not observed above 1.8 K for x = 0.20. Based on these results, the magnetic phase diagram for the Co-rich side of the $NdCoAsO-NdFeAsO$ system is constructed.

PACS numbers:

I. INTRODUCTION

Interest in Co containing 1111-type materials developed after Co was demonstrated to be an effective dopant to produce superconducting Fe-based 1111- and 122-materials [1, 2]. In the solid solution between NdCoAsO and NdFeAsO, spin density wave (SDW) ordering of Fe moments present in the Fe endmember is suppressed by Co substitution, resulting in superconductivity for Co concentrations of $5-20\%$, with maximum T_c of 6.5 K for 12% Co [3]. Similar results have been obtained for Co doping in LaFeAsO [1], CeFeAsO [4], PrFeAsO [5], and SmFeAsO [6, 7]. To date, phase diagram studies in Co-containing 1111-systems have been limited to these low Co concentrations, where superconductivity is found.

Similar to LnFeAsO (Ln = lanthanide), Co-based 1111-materials display interesting magnetic behavior, although the Co magnetism is quite different than the SDW antiferromagnetism found in the Fe compounds. LaCoAsO is a layered itinerant ferromagnet [1, 8], and other 1111-type materials LnCoAsO with magnetic lanthanides undergo multiple magnetic phase transitions involving both Co and Ln moments [3, 9–11]. In Nd-CoAsO, Co moments order ferromagnetically at $T_C = 69$ K, and two antiferromagetic transitions occur at lower temperatures. At $T_{N1} = 14$ K, the ferromagnetic Co moments rearrange into a layered antiferromagnetic structure, with simultaneous ordering of small moments on Nd. At $T_{N2} = 3.5$ K "full" moments on Nd order in the same magnetic structure [3, 11].

To construct the full phase diagram of the Co-substituted 1111-materials, it is necessary to study how the Co-related magnetism evolves as Co is replaced by Fe, and determine, for example, how far the ferromagnetic phase extends into the solid solution. Here we investigate the Co rich side of the $NdCoAsO-NdFeAsO$ system, and show how Fe substitution for Co suppresses the magnetism present in NdCoAsO. Polycrystalline samples of $NdCo_{1-x}Fe_xAsO$ were characterized by powder X-ray diffraction, electrical resistivity, and magnetization measurements. The effects of Fe substitution on the room temperature crystal structure are described, and the magnetic phase diagram for x $\leq$ 0.20 is presented.

II. EXPERIMENTAL DETAILS

Polycrystalline samples were synthesized similarly to our previous reports for NdFeAsO [12] and Nd-CoAsO [11]. Cold-pressed pellets with compositions $NdCo_{1-x}Fe_xAsO$ with x = 0.05, 0.10, 0.15, and 0.20 were fired in silica tubes at temperatures of $1100-1200$ °C for $12-24$ h. Powder X-ray diffraction (PXRD) patterns were collected using a PANalytical X'pert PRO MPD at room temperature using Cu-Kα_1 radiation. Rietveld refinements were carried out in the space group $P4/nmm$ using the program FullProf [13]. The eighteen fitted parameters include: unit cell parameters, z-coordinates of Nd and As, scale factors, preferred orientation, background coefficients, peak shape and half-width parameters, and sample displacement. Quantitative phase analysis indicate the samples to be about 95 % pure, with $Nd(SiO_4)O$ as the only detected impurity, resulting from reaction with the silica ampoules. Electrical resistivity measurements were performed using a Quantum Design Physical Properties Measurement System. Magnetization measurements were performed using a Quantum Design Magnetic Properties Measurement System. Semi-quantitative elemental analysis was carried out using energy dispersive X-ray analysis in a JEOL JSM-840 scanning electron microscope, and the Fe content determined from an average of four measurements on different crystallites.

III. RESULTS AND DISCUSSION

A. Crystal structure

Refined structural parameters are listed in Table I, and the dependence of unit cell volume and selected bonding data on the Fe content x are displayed in Fig-

TABLE I: Refined structural parameters from Rietveld analysis of room temperature PXRD data for $NdCo_{1-x}Fe_xAsO$. Data for NdCoAsO from Ref. [11].

x	a (Å)	c (Å)	z_{As}	z_{Nd}
0.00	3.98423(8)	8.3333(3)	0.6501(3)	0.1422(2)
0.05	3.98348(8)	8.3356(2)	0.6497(6)	0.1420(3)
0.10	3.98104(7)	8.3500(2)	0.6507(5)	0.1420(3)
0.15	3.97932(7)	8.3643(2)	0.6516(5)	0.1418(3)
0.20	3.97720(7)	8.3792(2)	0.6517(5)	0.1415(3)

ure 1. Like the end-members NdCoAsO and NdFeAsO, $NdCo_{1-x}Fe_xAsO$ adopts the ZrCuSiAs crystal structure in the space group $P4/nmm$ with Nd at $(\frac{1}{4}, \frac{1}{4}, z_{Nd})$, Co/Fe at $(\frac{3}{4}, \frac{1}{4}, \frac{1}{2})$, As at $(\frac{1}{4}, \frac{1}{4}, z_{As})$, and O at $(\frac{3}{4}, \frac{1}{4}, 0)$. The Fe content x determined from energy dispersive spectroscopy were within ± 0.03 of the nominal values for all samples, and within the expected uncertainty of the measurements. Due to the similar x-ray scattering factors of Co and Fe, the parameter x was not refined.

As Table I and Figure 1a show, the lattice constant a decreases as Fe replaces Co, while c and the unit cell volume increases. These same trends have been shown to continue on Fe rich side of the series [3]. As a result of the decrease in a, the increase in c, and the increase in the z-coordinate of As (Table I) with increasing x, the tetrahedra of As coordinating the transition metal (T) site becomes more regular, as shown by the As$-T-$As bond angles in Figure 1c. The T-centered tetrahedra remain flattened along the c-axis across the entire solid solution [3], the coordination being closest to ideal for the Fe end-member [14]. The $T-$As bond distance is smallest for the pure cobalt compound, and increases with x. This observation is consistent with the structural properties of binary arsenides, in which longer Fe$-$As distances, compared to Co$-$As, are found in isostructural compounds [15].

B. Physical Properties

Figure 2 shows the results of temperature dependent magnetization (M) and electrical resistivity (ρ) measurements. Effects of the magnetic phase transitions are observed in both of these properties. This allows the magnetic phase transition temperatures in $NdCo_{1-x}Fe_xAsO$ to be followed as x is varied.

Upon cooling into the ferromagnetic state, a strong increase in M is observed at T_C, where small moments on Co become aligned ferromagnetically. This occurs at 69 K in NdCoAsO, and is moved to lower temperatures as x is increased up to x = 0.15. No ferromagnetic transition is detected above 1.8 K for x = 0.20. The resistivity of NdCoAsO shows a subtle kink at T_C (best observed in dρ/dT, see Ref. [11]). This feature becomes more pronounced and moves to lower temperatures for x = 0.05 and 0.10. For x = 0.15, the resistive anomaly associated with T_C is not observed, likely due its proximity in tem-
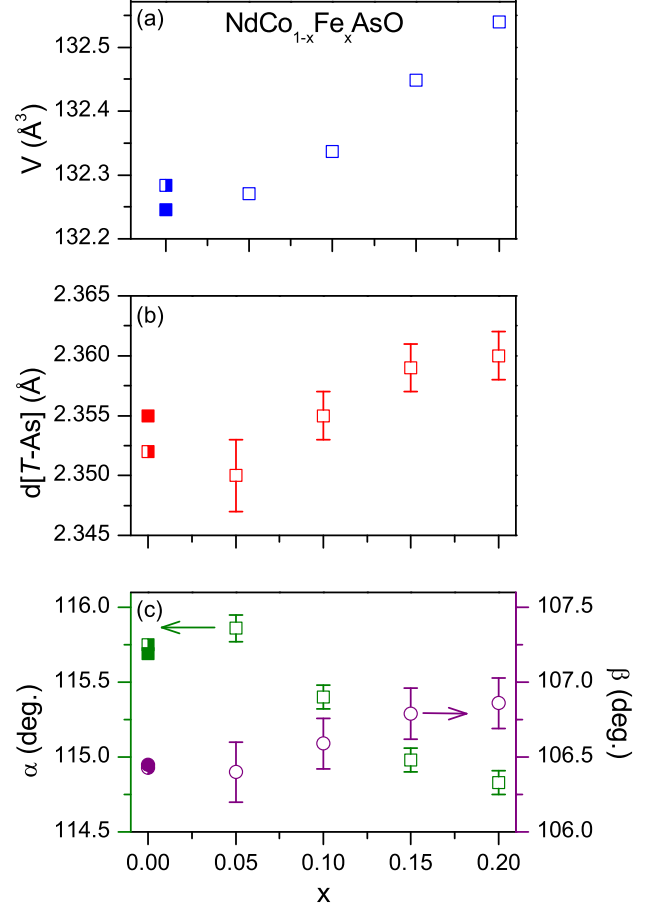

FIG. 1: (Color online) Selected structural information for $NdCo_{1-x}Fe_xAsO$: (a) unit cell volume, (b) $T-$As interatomic distance, (c) As$-T-$As bond angles. The angle α includes two As atoms on the same side of the T layer, while β includes As atoms on opposite sides of the T layer. Open symbols from current work. Half-filled points from Ref. [11]. Solid points from Ref. [3].

perature to the feature associated with T_{N1}. As noted for M, no anomalies in ρ are observed for x = 0.20.

At the ferromagnetic$-$antiferromagnetic transition temperature T_{N1}, M drops sharply as cobalt moments are rearranged to form an AFM stack of FM layers. In NdCoAsO, T_{N1} is near 14 K. Like T_C, T_{N1} is systematically decreased by Fe substitution. The transition in M is clearly observed for all samples except x = 0.20. At this transition, a sharp upturn in ρ is observed, indicating an effect on the magnetic scattering of the charge carriers, or changes in the electronic structure resulting from the magnetic transition. Like the resistivity feature at T_C, this anomaly at T_{N1} becomes more pronounced as Fe is substituted for Co, and is not observed for x = 0.20.

At T_{N2}, gradual downturns in both M and ρ are seen in NdCoAsO [11]. Suppression of T_{N2} upon Fe substitu-
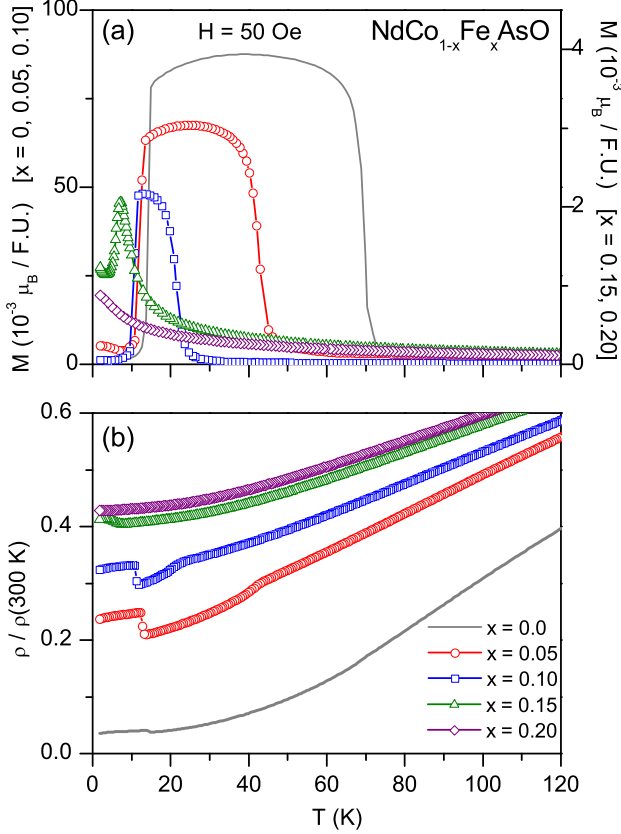
FIG. 2: (Color online)(a) Magnetization expressed in Bohr magnetons (μ_B) per formula unit (F.U.) from 1.8 to 120 K for $NdCo_{1-x}Fe_xAsO$. (b) Electrical resistivity vs. temperature from 1.8 to 120 K for $NdCo_{1-x}Fe_xAsO$, normalized at 300 K. Data for NdCoAsO from Ref. [11].

FIG. 3: (Color online) Magnetization vs. applied field for $NdCo_{1-x}Fe_xAsO$. For each composition, data are shown at 2 K and at a temperature near the maximum in magnetization in Figure 2a. Data for NdCoAsO are from Ref. [11]. Data were collected upon decreasing the applied field. Because no evidence of ferromagnetism is observed for x = 0.20 (Figure 2a), only data collected at 2 K are shown in (e).

tion to temperatures near or below the lower limit of this study (1.8 K) preclude the observation of these features even in the most lightly doped sample in the series (x = 0.05). In NdCoAsO, this transition is best observed in neutron diffraction and heat capacity [11]. Low temperature heat capacity measurements (not shown) on the Fe containing samples examined here confirmed that the peak associated with T_{N2} is suppressed as x is increased, and occurs at T ≤ 1.8 K for all nonzero values of x studied.

As illustrated in Figure 2b, the residual resistivity ratio increases as x increases. This may be attributed to the increase in disorder as more Fe replaces Co.

In NdCoAsO and other Co 1111-compounds, a small rapidly saturating component of the magnetization is observed in M vs. H plots at temperatures between T_C and T_{N1} [3, 10, 11]. These data are shown for $NdCo_{1-x}Fe_xAsO$ in Figure 3. Data were collected at temperatures where M is near its maximum value in Figure 2a, and at 2 K. Clearly, for x < 0.20, a ferromagnetic component is present at the magnetization maxi-
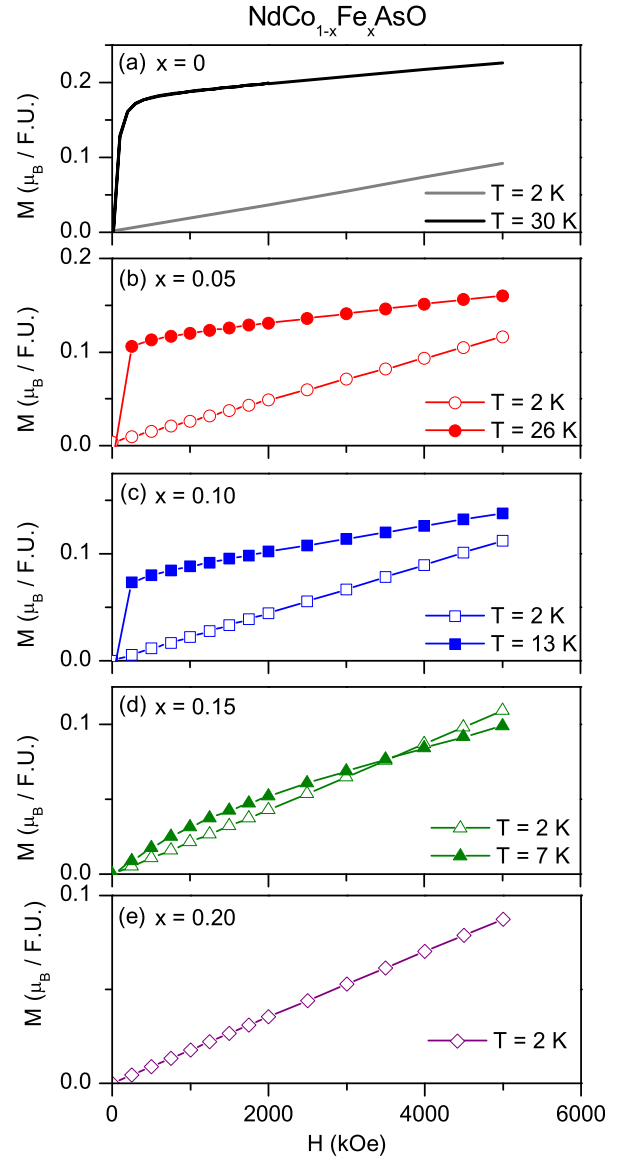
mum which is not present at 2 K. The linear behavior at higher fields is due to Nd paramagnetism.

As increased amounts of Fe are substituted for Co, the magnetism becomes increasingly weak, as evidenced by the lower transition temperatures and the smaller saturation moments. Because of this, and the closely spaced transition temperatures, it is difficult to resolve the transitions at T_C and T_{N1} in $\rho(T)$ and M(T) data for $x = 0.15$ (Figure 2). To confirm the presence of both transitions in this material, M(H) curves were collected at

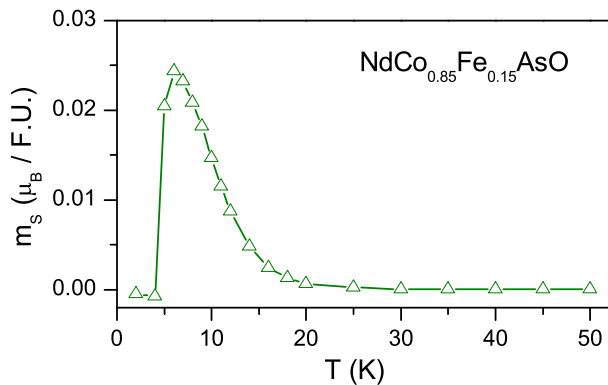FIG. 4: (Color online) Magnitude of the saturation component of the magnetic moment (m_S) of NdCo$_{0.85}$Fe$_{0.15}$AsO determined from M(H) measurements at temperatures between 2 and 50 K.

Curie temperature and the saturation moment per formula unit.
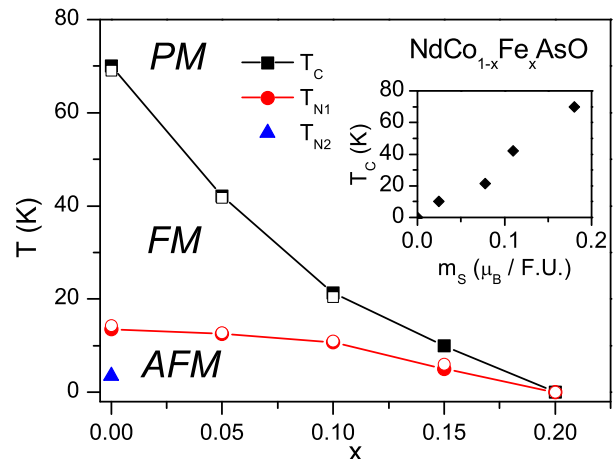

FIG. 5: (Color online) Magnetic phase diagram for the Co-rich side of the NdCo$_{1-x}$Fe$_x$AsO system showing the paramagnetic (PM), ferromagnetic (FM), and antiferomagnetic (AFM) regions. Solid symbols are from magnetization measurements (Figure 2a), and open symbols are from resistivity measurements (Figure 2b). For x = 0.20, no phase transitions are observed above 1.8 K. The inset shows the relationship between the Curie temperature T_C and the saturation moment (m_S).

temperatures between 2 and 50 K, and the saturation component was examined. The results are shown in Figure 4, and clearly show the development of a ferromagnetic component upon cooling through T_C and its abrupt disappearance at T_{N1}.

Using the transport and magnetization results in Figures 2 and 4, the magnetic phase diagram of the NdCoAsO−NdFeAsO system near the Co endmember is constructed and shown in Figure 5. Transition temperatures were determined from the extrema in the temperature derivatives of the measured resistivity and magnetization (saturation moment for $x = 0.15$), which estimates the midpoint of the observed anomalies. Although this is an unorthodox method for treating magnetization data, it provides a simple and consistent means of defining the transition temperatures from both resistivity and magnetization measurements. Note that the resistivity anomaly associated with T_C is not resolved for x = 0.15. In addition, T_{N2} was not observed in resistivity and magnetization for any of the Fe containing samples, and is shown only for x = 0. As noted above, heat capacity measurements confirm $T_{N2} \leq 1.8$ K for $x \geq 0.05$.

Figure 5 shows that T_C is suppressed more rapidly than T_{N1} as Fe is substituted for Co. This is perhaps due to fact that the FM transition likely involves only transition metal moments, while Nd is also involved in the AFM transition. As a result, both of these magnetic phase transitions are suppressed to below 1.8 K near the same critical Fe concentration between 15 and 20 %.

Linear fits to the M vs. H data shown in Figure 3 were extrapolated to H = 0 to estimate the maximum saturation moments for each composition. The inset of Figure 5 shows the nearly linear relationship between the

IV. CONCLUSIONS

This work demonstrates that the solid solution which has been established on the Fe rich side of the NdCoAsO−NdFeAsO system [3] continues to the Co-rich side. Small amounts of Fe (5−20%) were successfully substituted for Co, and the effects on the crystal structure, electrical transport, and magnetization were determined. X-ray diffraction results show a smooth variation of the structural parameters as Fe replaces Co, following the same trends that are observed near NdFeAsO (Fig. 1). Resistance and magnetization measurements allow the construction of the magnetic phase diagram near NdCoAsO shown in Figure 5. The results show that both T_C and T_{N1} are suppressed below 1.8 K near the same Fe concentration between 15 and 20%, and suggest that T_{N2} is suppressed at much lower Fe concentrations ($\lesssim 5\%$). The relationship between T_C and the saturation moment in the FM phase was found to be nearly linear.

[1] A. S. Sefat, A. Huq, M. A. McGuire, R. Jin, B. C. Sales, D. Mandrus, L. M. D. Cranswick, P. W. Stephens, and K. H. Stone, Phys. Rev. B **78**, 104505 (2008).

[2] A. S. Sefat, R. Y. Jin, M. A. McGuire, B. C. Sales, D. J. Singh, and D. Mandrus, Phys. Rev. Lett. **101**, 117004 (2008).

[3] A. Marcinkova, D. A. M. Grist, I. Margiolaki, T. C. Hansen, S. Margodonna, and J.-W. G. Bos, Phys. Rev. B **81**, 064511 (2010).

[4] J. Prakash, S. J. Singh, S. Patnaik, and A. K. Ganguli, Solid State Commun. **149**, 181 (2009).

[5] P. Shirage, K. Miyazawa, H. Kito, H. Eisaki, , and A. Iyo, Physica C **469**, 898 (2009).

[6] C. Wang, Y. K. Li, Z. W. Zhu, S. Jiang, X. Lin, Y. K. Luo, S. Chi, L. J. Li, Z. Ren, M. He, et al., Phys. Rev. B **79**, 054521 (2009).

[7] A. Pal, M. Husain, H. Kishan, and V. Awana, arXiv:1007.5121.

[8] H. Ohta and K. Yoshimura, Phys. Rev. B **79**, 184407 (2009).

[9] V. P. S. Awana, I. Nowik, A. Pal, K. Yamaura, E. Takayama-Muromachi, and I. Felner, Phys. Rev. B **81**, 212501 (2010).

[10] H. Ohta and K. Yoshimura, Phys. Rev. B **80**, 184409 (2009).

[11] M. A. McGuire, D. J. Gout, V. O. Garlea, A. S. Sefat, B. C. Sales, and D. Mandrus, Phys. Rev. B **81**, 104405 (2010).

[12] M. A. McGuire, R. P. Hermann, A. S. Sefat, B. C. Sales, R. Jin, D. Mandrus, F. Grandjean, and G. J. Long, New J. Phys. **11**, 025011 (2009).

[13] J. Rodriguez-Carvajal, Physica B **192**, 55 (1993), program available at www.ill.fr/dif/Soft/fp/.

[14] Y. Qiu, W. Bao, Q. Huang, T. Yildirim, J. M. Simmons, M. A. Green, J. Lynn, Y. C. Gasparovic, J. Li, T. Wu, et al., Phys. Rev. Lett. **101**, 257002 (2008).

[15] P. S. Lyman and C. T. Prewitt, Acta Crystallogr. B **40**, 14 (1984).